

Dynamics of condensate formation in stochastic transport with pair-factorized steady states: Nucleation and coarsening time scales

Hannes Nagel* and Wolfhard Janke†

Institut für Theoretische Physik, Universität Leipzig, Postfach 100 920, 04009 Leipzig, Germany

Driven diffusive systems such as the zero-range process (ZRP) and the pair-factorized steady states (PFSS) stochastic transport process are versatile tools that lend themselves to the study of transport phenomena on a generic level. While their mathematical structure is simple enough to allow significant analytical treatment, they offer a variety of interesting phenomena. With appropriate dynamics, the ZRP and PFSS models feature a condensation transition where for a supercritical density the translational symmetry breaks spontaneously and excess particles form a single-site or spatially extended condensate, respectively. In this paper we numerically study the typical time scales of the two stages of this condensation process: Nucleation and coarsening. Nucleation is the first stage of condensation where the bulk system relaxes to its stationary distribution and droplet nuclei form in the system. These droplets then gradually grow or evaporate in the coarsening regime to finally coalesce in a single condensate when the system finally relaxes to the stationary state.

We use the ZRP condensation model to discuss the choice of the estimation method for the nucleation time scale and present scaling exponents for the ZRP and PFSS condensation models with respect to the choice of the typical droplet nuclei mass. We then proceed to present scaling exponents in the coarsening regime of the ZRP for partially asymmetric dynamics and the PFSS model for symmetric and asymmetric dynamics.

I. INTRODUCTION

Stochastic transport processes have been studied for a long time to understand fundamental principles in various physical and non-physical systems on a wide range of length-scales. Originally introduced to study properties of interacting Markov processes by Spitzer [1], they were found to be versatile enough to provide mappings or models of more realistic systems. For instance, extended versions of the asymmetric exclusion process and related models have been used to model intracellular locomotion of molecular motors [2] as well as vehicular and other traffic [3–5]. To us, another interesting field of application is the modeling and understanding of general condensation phenomena that are observed in a broad range of physical systems, such as colloidal and granular systems [6], the formation of breath figures [7], the condensation on inhomogeneous networks [8–10], the aggregation of links in networks [11] as well as in a variety of other contexts [3, 5, 12]. Some stochastic transport processes, in general driven far from equilibrium, lend themselves to this domain due to their relative simplicity, the occurrence of phase separation and the resulting rich phase structures being present already in one dimension [13]. For example, the asymmetric simple exclusion process (ASEP) features a phase diagram with a maximum current, as well as a low-density and a high-density phase induced by externally driven particle exchange at the system boundaries [14–18]. Another well-known example for the occurrence of phase separation in a one-dimensional stochastic transport model is the zero-range

process (ZRP) [1, 13, 19, 20], where particles on the same site interact non-exclusively: With appropriate dynamics, this model features a condensation transition with a coexisting localized particle condensate and a “fluid” background or bulk phase. For sufficiently high particle density ρ , the translational symmetry breaks down spontaneously and a condensate containing a finite fraction of particles emerges at a single site in the system while the remaining particles form the bulk of the system. This condensation model within the ZRP has been extensively discussed in the literature, so that a wide host of properties is well known and many related models were proposed and studied. For example, a model with nearest-neighbour interactions proposed by Evans et al. [21] features formation of spatially extended condensates, a property the ZRP lacks due to its interaction range being zero. In this model, the stationary state factorizes over lattice bonds instead of sites as for the ZRP, which is why it is often referred to as the pair-factorized steady states (PFSS) model, mainly to distinguish from the fully factorized steady state of the ZRP. Many stationary properties of the condensed state in this family of models such as the condensate’s shape and length scale [22–24], mobility [25, 26], metastability of the condensate [27] or boundary induced phase separation [28–30] were studied.

Besides these interesting stationary properties of the condensed state of these models, the dynamics that lead to it are of interest to the study of general condensation phenomena. In this paper we will discuss the dynamics of the condensation process for the PFSS model as well as the ZRP. Specifically we will determine and discuss the time scales of the two main steps of the relaxation process from a random initial state to the final stationary distribution where a single condensate contains the entire excess particles of the system. These general steps

* Hannes.Nagel@itp.uni-leipzig.de

† Wolfhard.Janke@itp.uni-leipzig.de

are the *nucleation* and *coarsening* processes as in the well-known picture of Ostwald ripening [31]. Classical theories of precipitation in this context are the Szilard–Farkas and Becker–Döring models [32, 33] for nucleation and the Lifshitz–Slyozov–Wagner model [34] in the coarsening regime. Nucleation is the initial diffusive accumulation of several particles to small droplets that are larger than the typical fluctuations in the critical background of the relaxed system. Coarsening refers to the growth of some droplets and the evaporation of smaller ones until only a single large droplet persists and the steady state is reached. While the steady state might be in non-equilibrium due to an external drive and particle transport, this process irreversibly relaxes the system from a non-equilibrium state towards the stationary distribution. The time scale of these processes refers to the dependence of the nucleation and coarsening times to the size of the system.

For the ZRP, the nucleation and coarsening steps and the corresponding time scales have been treated analytically for symmetric as well as totally asymmetric dynamics by Grosskinsky et al. [35]. In an earlier study the coarsening time scale of a finite ZRP has been determined by interpreting the size of the largest condensate as a bounded and biased random walk and calculating the first-passage time when the largest condensate absorbed any particles of a smaller condensate [25, 36].

In this article we will extend these considerations for the ZRP to the generalized PFSS condensation model proposed by Evans et al. [21] featuring short-range interactions. While this allows us to create more realistic models of transport phenomena, its mathematical structure remains simple and similar to the ZRP. Most importantly here is, that the introduction of nearest-neighbour interactions allows the emergence of spatially extended condensates. In fact, variations of the hopping dynamics have been proposed that lead to interesting properties of the condensate, such as a tunable envelope shape and scaling of the condensate width [22–24]. In a recent contribution we discussed another variant as a toy model in the context of thin film growth [37], where the system starts empty and condensation gradually takes place as particles are deposited from the outside. We are therefore interested in comparing the nucleation and coarsening processes of extended droplets in this model to those observed in the ZRP and specifically determine the respective time scales.

We will continue as follows. We first introduce the ZRP and PFSS models and discuss the expected time scales in Sec. II. In the following Sec. III, we discuss the numerical methods employed to simulate the dynamics and track the condensation process. We will further describe our considered methods to compute the time scale exponents from the trajectories. In Secs. IV and V, we compare our results for the condensation time scales of the ZRP and PFSS processes respectively. Finally, the last Sec. VI contains the conclusions of our work.

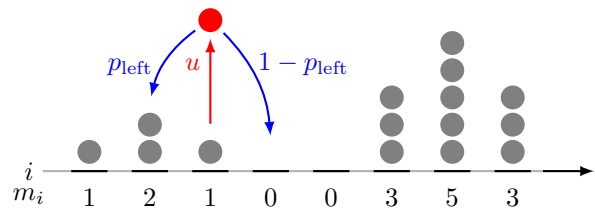


FIG. 1. Schematics of the discussed models. From a randomly selected site i a particle is taken with probability $u_{\text{ZRP}} = u(m_i)/u_{\text{max,ZRP}}$ or $u_{\text{PFSS}} = u(m_i|m_{i-1}, m_{i+1})/u_{\text{max,PFSS}}$, and then moved to sites $i-1$ or $i+1$ with probability p_{left} or $1-p_{\text{left}}$, respectively.

II. MODELS

We consider condensation phenomena in two related models of stochastic transport processes: The zero-range process (ZRP) and the pair-factorized steady states (PFSS) model. The ZRP is a minimal model of a particle-hopping stochastic transport process with local interactions only. The PFSS model introduces nearest-neighbour interactions additionally to the zero-range interactions of the ZRP. We will use the simpler ZRP to setup and validate our methods to estimate the time scales of the condensation process in the latter model.

In both models the system consists of a number of indistinguishable particles that occupy the sites of a lattice or graph. The number of particles occupying a specific site i is called the occupation number m_i and can be any integer value $0 \leq m_i \leq M$, where $M = \sum_{i=1}^L m_i = \rho L$ is the total particle number in a system of L sites. At every step of the stochastic process a site i in the lattice is randomly selected for trial of particle hopping. If the site is occupied, hopping of a single particle succeeds with the hopping rate u per unit time and the particle hops to a neighbour of its departure site. Random choice of the hopping target leads to an equilibrium system, while a biased choice can lead to a system driven far from equilibrium. We will consider the case of the one-dimensional periodic lattice, where such a drive is easily implemented by a probability p_{left} of the particle to hop to the nearest neighbour in negative direction of the lattice and in positive direction with probability $1-p_{\text{left}}$. For any given lattice and number of particles M the individual dynamics of the particles in these models are therefore fully described by the hopping rate function and the strength of the bias in the hopping direction. The general update scheme of this family of processes is given in Fig. 1.

A. The zero-range process

The ZRP was originally proposed to model a set of non-exclusively interacting random walks by Spitzer [1]. It is constructed to be analytically tractable and has, for symmetric as well as asymmetric dynamics, always the

same factorised stationary distribution

$$P_{\text{ZRP}}(\{m\}) = \frac{1}{Z_{\text{ZRP}}^{M,L}} \left(\prod_{i=1}^L p(m_i) \right) \delta_{\sum_{i=1}^L m_i, M}, \quad (1)$$

where $\{m\} = (m_1, \dots, m_L)$ is a specific configuration of the system. The factorisation of the steady state is carried out over the single-site weight functions $p(m)$ for all sites. The normalisation constant $Z_{\text{ZRP}}^{M,L}$ used here has the same role as the partition function in an equilibrium model and the Kronecker symbol $\delta_{\sum_{i=1}^L m_i, M}$ ensures the conservation of particles. With the choice of the weight function

$$p(m) = \prod_{n=1}^m \left(\frac{1}{u(n)} \right), \quad p(0) = 1 \quad (2)$$

the hopping rate function then becomes

$$u(m) = \frac{p(m-1)}{p(m)}. \quad (3)$$

It is easy to check that this leads to the steady state (1) by inserting (2) and (3) into the master equation

$$\frac{\partial}{\partial t} P(\{m\}) = 0 = \sum_{\{m'\}} \left[W(\{m'\} \rightarrow \{m\}) P(\{m'\}, t) - W(\{m\} \rightarrow \{m'\}) P(\{m\}, t) \right], \quad (4)$$

where the transition rates are $W(\{m\} \rightarrow \{m'\}) = u(m_i)p_{\text{left}}$ for a hop to the left ($\{m'\} = \{m_1, \dots, m_{i-1} + 1, m_i - 1, \dots, m_L\}$), $W(\{m\} \rightarrow \{m'\}) = u(m_i)(1 - p_{\text{left}})$ for a hop to the right ($\{m'\} = \{m_1, \dots, m_i - 1, m_{i+1} + 1, \dots, m_L\}$), and $W(\{m\} \rightarrow \{m'\}) = 0$ otherwise.

In this work we consider the well-known ZRP condensation model [13, 19] with hopping rate function

$$u(m) = 1 + \frac{b}{m}. \quad (5)$$

For this choice of dynamics, condensation occurs for $b > 2$ above a critical density of $\rho_c = 1/(b-2)$. When the total number of particles is increased above the condensation threshold $M > \rho_c L$, the translational symmetry breaks down and the excess particles $M' = M - \rho_c L$ condense at a single site in the system. The occupation number of the rest of the system remains on average at the critical density ρ_c . For illustration, the average mass of the largest droplet $M'(t)$ during a complete condensation is shown in Fig. 2 for a number of system sizes with totally asymmetric dynamics. Note, how for small times, the largest droplets grow very similarly, while coarsening takes much longer for larger lattices.

The scaling of the nucleation and coarsening times as determined by Grosskinsky et al. [35] assumes a power-law in the system size of the form

$$\tau = aM^\delta, \quad (6)$$

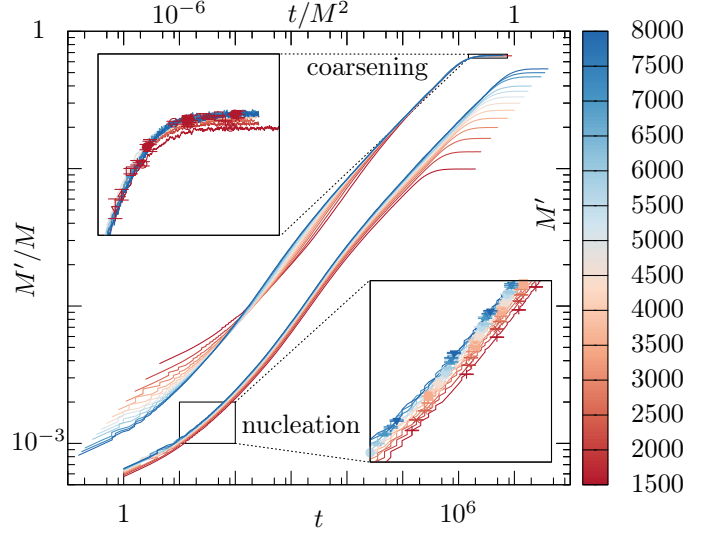


FIG. 2. The nucleation (bottom right) and coarsening (top left) processes for various system sizes in the ZRP as observed in the average mass of the largest droplet at time t . The two groups of curves show the same data. The upper group, plotted versus the top and left axes, is merely rescaled in time by $1/M^2$ and in mass by $1/M$ in order to collapse the trajectories of different system sizes to a single master curve for late times, as shown in the upper inset. The lower group, plotted versus the lower and right axes, is shown without rescaling. The lower inset shows the weak dependence of droplet growth on system size in the early condensation dynamics. The curves were determined for totally asymmetric dynamics $p_{\text{left}} = 1$ using 1000 trajectories per size $L = M$.

that is also observed for other relaxation processes in the ZRP with different dynamics [38]. To estimate the nucleation time scale, Grosskinsky et al. propose a mass threshold m_t for a droplet nuclei and calculate the time it takes to populate the system with such nuclei. For the choice of a threshold linear in the system size $m_{t,\text{lin}} = \alpha_{\text{lin}}(\rho - \rho_c)L$, with some constant $\alpha \ll 1$, they estimate the scaling exponent of the nucleation time as $\delta_{\text{nuc},\text{ZRP}} = 3$ for symmetric ($p_{\text{left}} = 1/2$) and $\delta_{\text{nuc},\text{ZRP}} = 2$ for totally asymmetric ($p_{\text{left}} = 1$) dynamics. The coarsening time is dominated by the typical time for a droplet to loose all particles, which is determined using the fact that for the ZRP the evaporation rate of a droplet is simply the hopping rate for the droplet mass.

B. The PFSS transport process

The basic PFSS short-range interaction transport process differs from the ZRP by taking the interactions between particles on adjacent sites into account. This is realized by replacing the single-site weight $p(m)$ of the ZRP with a two-point weight function $g(m, n)$ for each bond in the system. The stationary distribution of this

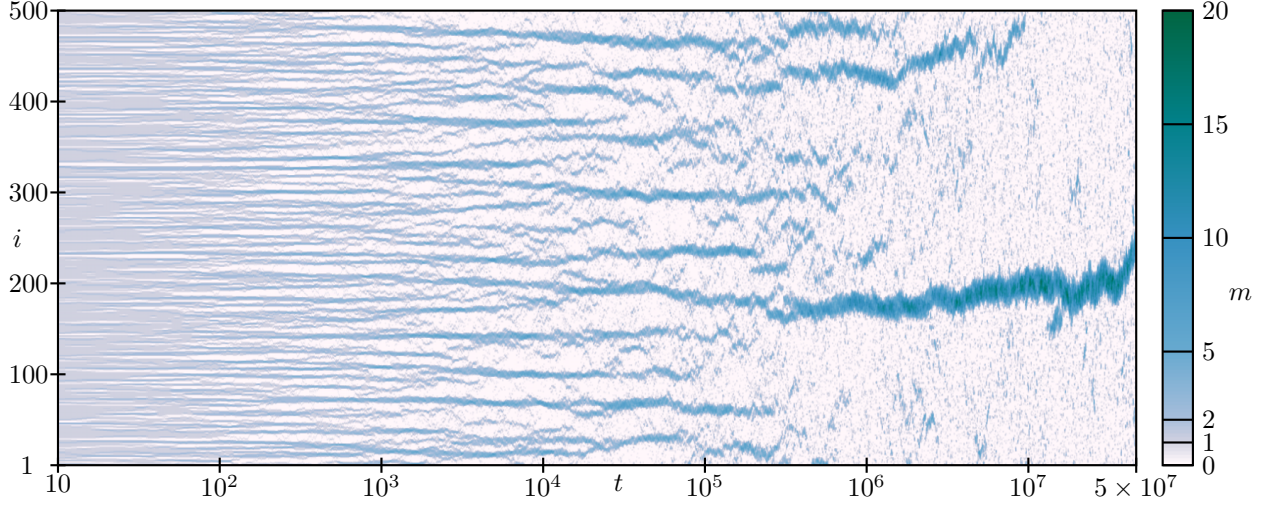


FIG. 3. Sample time series of a PFSS condensation process in a system of $L = 500$ sites and $M = 500$ particles for totally asymmetric dynamics ($p_{\text{left}} = 1$, “particles cyclically move down”) and interaction parameters $U = J = 1$. Each vertical slice in the plot corresponds to the occupation number vector at time t . The time axis is logarithmic to show the different stages of the condensation process. Starting with a disordered state in the leftmost slice, small droplets emerge and gradually coarsen on every time scale until a single condensate remains at about $t \approx 10^7$.

process then assumes the form

$$P(\{m\}) = \frac{1}{Z_{\text{PFSS}}^{M,L}} \prod_{i=1}^L g(m_i, m_{i+1}) \delta_{\sum_{i=1}^L m_i, M}, \quad (7)$$

i.e. it factorizes over pairs of sites, giving rise to the name *pair-factorized steady states (PFSS)* transport process. Here the bond weight function $g(m, n)$ is a positive and in our case symmetric function. The corresponding hopping rate function that controls the dynamics of the process is determined similarly as for the ZRP using the master equation (4) with appropriate transition rates $W(\{m\} \rightarrow \{m'\}) = u(m_i | m_{i-1}, m_{i+1}) p_{\text{left}}$ for a hop to the left ($\{m'\} = \{m_1, \dots, m_{i-1} + 1, m_i - 1, \dots, m_L\}$), $W(\{m\} \rightarrow \{m'\}) = u(m_i | m_{i-1}, m_{i+1}) (1 - p_{\text{left}})$ for a hop to the right ($\{m'\} = \{m_1, \dots, m_i - 1, m_{i+1} + 1, \dots, m_L\}$), and $W(\{m\} \rightarrow \{m'\}) = 0$ otherwise. The resulting hopping rate function is then given by

$$u(m_i | m_{i-1}, m_{i+1}) = \frac{g(m_i - 1, m_{i-1})}{g(m_i, m_{i-1})} \frac{g(m_i - 1, m_{i+1})}{g(m_i, m_{i+1})}. \quad (8)$$

A compelling general choice of the bond weight is to use the factorized form $g(m, n) = \sqrt{p(m)p(n)} K(|m - n|)$, with a zero-range site weight function $p(m)$ as in the ZRP and a short-range part $K(x)$. Thus, the ZRP is easily reproduced as a special case by setting $K(x) \equiv 1$ and a broad range of interactions can be implemented by interpreting the partial weights $p(m)$ as a particle-site potential and $K(|m - n|)$ as a particle-particle interaction term. Due to the ranged interactions there is now the possibility that spatially extended condensates emerge in the system. A number of specific weights and thus dynamics have been considered in the literature for this

model, such as that suggested in its original proposition by Evans et al. [21] or the tunable interactions resulting in various condensate shapes [22–24].

The main question that we are going to resolve in this work, is whether the nucleation and coarsening dynamics of condensation in this model with short-range interactions takes place on the same time scale as for the ZRP. To do this, we will consider the dynamics suggested in Ref. [21] given by the partial weights

$$p(m) = e^{U\delta_{m,0}}, \quad K(x) = e^{-Jx}. \quad (9)$$

Here, U gives the strength of an on-site potential and J can be interpreted as a surface energy. In this work, we will only explicitly discuss the case $U = 1, J = 1$, although we did check different parametrisations as well as different dynamics with pair-factorized steady states featuring condensation. Inserting this into the Eq. (8) gives the hopping rate function

$$u(m_i | m_{i-1}, m_{i+1}) = \begin{cases} e^{-2J+U\delta_{m_i,1}} & m_i \leq m_{i-1}, m_{i+1}, \\ e^{2J+U\delta_{m_i,1}} & m_i > m_{i-1}, m_{i+1}, \\ e^{U\delta_{m,1}} & \text{otherwise.} \end{cases} \quad (10)$$

As an illustration of this dynamics, Fig. 3 shows a time series of configurations from a random initial state to the stationary state with a single condensate.

For this choice of dynamics the critical density can be determined as $\rho_c = 0.2397$ for parameters $U = 1, J = 1$ [22]. Above this density an extended condensate of roughly parabolic shape containing the excess particles $(\rho - \rho_c)L$ emerges. The exact shape can be determined as well [23]. The extension of the condensate scales as the square root of its mass M' for sufficiently large systems [21, 22]. Because of the spatial extension as well as

the smooth shape of the droplets, and ultimately the remaining single condensate, it is non-trivial to reproduce either the analytical or the qualitative arguments for the nucleation and coarsening time scales in this case. Therefore, in this work, we perform numerical simulations of both the ZRP and PFSS model to calibrate our methods by the ZRP results and determine the time-scale exponents for the PFSS process using the power-law ansatz (6) as for the ZRP.

III. NUMERICAL SIMULATIONS

We employ a kinetic Monte Carlo method with discrete time steps that directly simulates the dynamics of the considered transport processes. Per time step, every lattice site is considered on average once for a local update that consists of the following steps: A site i with $1 \leq i \leq L$ is randomly and uniformly chosen and, if occupied, the hopping rate u_i for that site is determined according to (5) or (10). A particle leaves the site, with the probability u_i/u_{\max} , where

$$u_{\max} = \begin{cases} b+1 & \text{ZRP} \\ e^{2J+U} & \text{PFSS for } U, J > 0 \end{cases} \quad (11)$$

is the maximal hopping rate for the given model. The particle then enters the left ($i-1$) or right ($i+1$) neighbour with probability p_{left} and $1-p_{\text{left}}$, respectively. At the boundary sites $i=1, L$ we consider periodic boundary conditions, so that the left neighbour of the first site and the right neighbour of the last site are identified as the last and first site respectively. Because of the definition of the hopping rate in events per physical time unit, a Monte Carlo *sweep* of L single-site updates corresponds to $1/u_{\max}$ units of physical time. By repeating this update procedure, a single trajectory of configurations $\{m\}(t)$ is generated.

In contrast to steady-state simulations, where an observable can be estimated from a large number of observations in a single trajectory, here every trajectory contributes only a single observation to the estimation of the typical nucleation and coarsening times. To determine a sufficiently good estimate for the scaling exponents we hence generated on the order of several thousand trajectories for every parametrisation.

IV. NUCLEATION

Nucleation is the first stage of the condensation process, covering the formation of particle droplet nuclei from the bulk system until the bulk phase is relaxed and coarsening takes over. Since the number of particles in the system $M = \rho L$ is conserved, the initial configuration is prepared using a uniform distribution of particles. For any supercritical density $\rho > \rho_c$ the system then contains

$(\rho - \rho_c)L$ excess particles that settle at random sites forming droplets. In the case of the ZRP, such a droplet is just a larger number of particles on a single site with respect to the occupation number distribution in the bulk of the system. The mass of a droplet, that is the number of contained particles, is therefore equal to the occupation number at its location for the ZRP. In the PFSS model, where droplets are in general extended, we require separation by at least one site with occupation below the critical density $m_i < \rho_c$, that is $m_i = 0$ in both models for the parameters considered in this paper. The sum of occupation numbers in the droplet region then defines its mass.

To gain a basic understanding of the involved time scales determining the nucleation process, we can somewhat generalize the heuristic approximation of the scaling exponent for the ZRP by Grosskinsky et al. [35]. When the typical cluster mass is assumed to be linear in the system size $\alpha(\rho - \rho_c)L$, it follows that there are on the order of $1/\alpha$ droplets in the system. The density of droplets in turn determines the average free distance that particles travel to a nuclei. The time, in units of single hops, for on the order of L particles to travel a distance of order L is then roughly L^2 for totally asymmetric dynamics and L^3 including diffusive motion due to symmetric dynamics. The choice of the typical droplet mass being linear in the system size ensures that droplets are distinctly larger than random fluctuations, which are of order $[\Gamma(b-1)L]^{1/(b-1)}$ for the ZRP [35], where $\Gamma(x)$ is the gamma function. However, assuming a different functional dependence of the typical droplet mass, such as a proportionality to the square root of the excess particles $\alpha_{\text{sqr}} \sqrt{(\rho - \rho_c)L}$, results in a change of the time scale as well: On the order of $L^{1/2}$ particles travelling for a mean free distance of order $L^{1/2}$ sites yields a time scale of order L for asymmetric and $L^{3/2}$ for symmetric dynamics.

Because of this, we will first reproduce and compare the time scale for nucleation in the ZRP before proceeding to the PFSS model. Furthermore, we will consider three types of typical droplet masses of the form

$$m_t = \begin{cases} \alpha_{\text{lin}}(\rho - \rho_c)L & m_{t,\text{lin}} \\ \alpha_{\text{sqr}} \sqrt{(\rho - \rho_c)L} & m_{t,\text{sqr}} \\ \text{const} & m_{t,\text{const}} \end{cases} \quad (12)$$

to check our former assumptions and compare the resulting kinetics. The additional threshold $m_{t,\text{const}}$ independent of the system size is motivated as follows. The critical droplet size in the nucleation regime is the size of a droplet for which its growth rate becomes faster than its decay rate. For the single-site droplets in the ZRP, we can determine this size by evaluating the droplet growth in the vicinity of the critical droplet size m_c

$$\left. \frac{\partial m}{\partial t} \right|_{m \approx m_c} = 0 = \sum_{n=1}^{\infty} P(m_{\pm 1} = n) u(n) - u(m_c), \quad (13)$$

where $P(m_{\pm 1} = n)$ is the probability to find n particles on the adjacent sites. As the bulk should relax within the nucleation time, we can assume that $P(m_{\pm 1} = n) = \pi(m)$ is the mass distribution of the ZRP, that is $\pi(m) = p(m) \exp(-\mu m)$ with the chemical potential μ in the grand-canonical system and thus $\pi(m) \propto p(m) \approx \Gamma(b+1)m!/\Gamma(b+1+m)$ for a fixed number of particles. We can now find the critical value as $m_c \approx b\Gamma(b-1)/[\Gamma(b-1) + \Gamma(b-2)]$ which is $m_c = 15/2$ for the interaction strength $b = 5$ used here and set our threshold including a small safety margin to $m_{t,\text{const}} = 10$.

To determine the nucleation time scale using numerical simulations, we will compute the transition time when the coarsening of droplets starts to dominate the kinetics of the system, that is the formation of new droplets of at least the typical mass m_t becomes smaller than the evaporation of existing ones. This is achieved by counting the number of droplets that have at least the typical mass (threshold mass) at every time in the trajectory and computing its average over many trajectories. The scaling exponent is then determined visually for the best data collapse assuming the power law (6).

A. ZRP

To compare with the results of Grosskinsky et al. [35] and validate our numerical methods, we use a similar parameter set with system sizes of $L = 320, 640, 1280$, and 2560 sites, interaction strength $b = 5$, yielding $\rho_c = 1/(b-2) = 1/3$, and somewhat more variation in the particle density $\rho = 1, 2, 4, 8$, and 12 . To compute the average droplet-count function $n_c(t)$ we simulated 1200 trajectories for each combination of parameters with totally asymmetric ($p_{\text{left}} = 1$) as well as symmetric ($p_{\text{left}} = 1/2$) dynamics. We then rescaled the average droplet counts to achieve a good collapse for different system sizes and get the scaling with respect to the mass thresholds (12).

Figure 4 shows that these results indeed reflect the heuristic approximations made for the different assumptions of the typical droplet mass m_t . The curves of the droplet counts collapse in two ways. Firstly, for identical values of the particle density ρ there is a collapse for individual system sizes L . Secondly, for the size-dependent thresholds and asymmetric dynamics, this collapse increases with the particle density and a common master curve is approached. For typical droplet masses $m_{t,\text{const}}$ independent of the system size, the collapse for different L within the same density is remarkable. While this might to some extent reflect the higher absolute value of droplet counts and thus greater amount of self-averaging in that situation, it also suggests that this assumption is indeed physical. The rescaling factors in the vertical axis for the mass thresholds $m_{t,\text{const}}$ and $m_{t,\text{sqrt}}$ reflect the respective expected number of droplets per system size according to the heuristic approximation. Comparing with Ref. [35], that is specifically for typical droplet

sizes $m_{t,\text{lin}} = \alpha_{\text{lin}}(\rho - \rho_c)L$ linear in the system size with $\alpha_{\text{lin}} = 1/40$, our value of the scaling exponent $\delta_{\text{nucl}} = 2$ is consistent with the value determined for the assumption therein.

While the droplet mass threshold in the original work by Grosskinsky et al. [35] is chosen to ensure that such droplets are distinct from fluctuations of order $[\Gamma(b-1)L]^{1/(b-1)}$ in the initial system for any value of the interaction strength b , our assumption $m_{t,\text{sqrt}}$ fulfills this requirement as well for the considered interaction strength of $b = 5$. Additionally, we performed a similar amount of simulations for $b = 4$ yielding very similar results. Considering that the data collapse for $m_{t,\text{sqrt}}$ and $m_{t,\text{lin}}$ is equally good, we would then suggest that, if the duration of the nucleation regime can be limited in this approach, the systematically smaller yet valid assumption of the typical droplet size should be physical.

Finally, as the third assumption for the typical droplet size $m_{t,\text{const}}$, we use our estimate of the critical droplet size for the ZRP $m_{t,\text{const}} = 10$ although it becomes smaller than the expected fluctuations in the initial configuration for larger systems. This is visible in Figs. 4(a,d), where for large densities the droplet count indeed approaches from higher values and does not reach a local maximum. Using a threshold with a larger margin to the critical droplet size, such as $m_{t,\text{const}} = 20$, mitigates this effect so that the droplet counts for large densities become similar to those for lower densities $\rho \leq 8$. Without any rescaling in time, the data collapse in the observed droplet counts for systems of different sizes is excellent within the same particle density.

Our results show that, in order to determine a meaningful time scale for the nucleation process using this method, it is crucial to carefully select a relation of the typical droplet mass m_t to the system size with respect to the considered system and to some extent the desired properties of the forming droplets. With respect to that, we only visually determined estimates of the nucleation exponents instead of performing extensive analysis to find numerical values for maximum overlap. A summary of the determined scaling exponents is given in Table I. Furthermore, we validated our numerical methods to proceed to the nucleation time of the PFSS model in the next section.

B. PFSS

For the PFSS we use a fixed set of interaction parameters $U = J = 1$ for the weights (9) and resulting hopping rate function (10). The remaining parameters are comparable to those for the ZRP with a range of system sizes of $L = 400, 800, 1600$, and 3200 sites and particle densities of $\rho = 1, 2$, and 4 . We use the same method as for the ZRP to determine the scaling exponents δ_{nucl} for the typical droplet sizes (12) with slightly larger constants $\alpha_{\text{lin}} = 1/20$ and $\alpha_{\text{sqrt}} = 5/2$ due to the lower critical density $\rho_c \approx 0.2397$ and the spatial extension of the droplets.

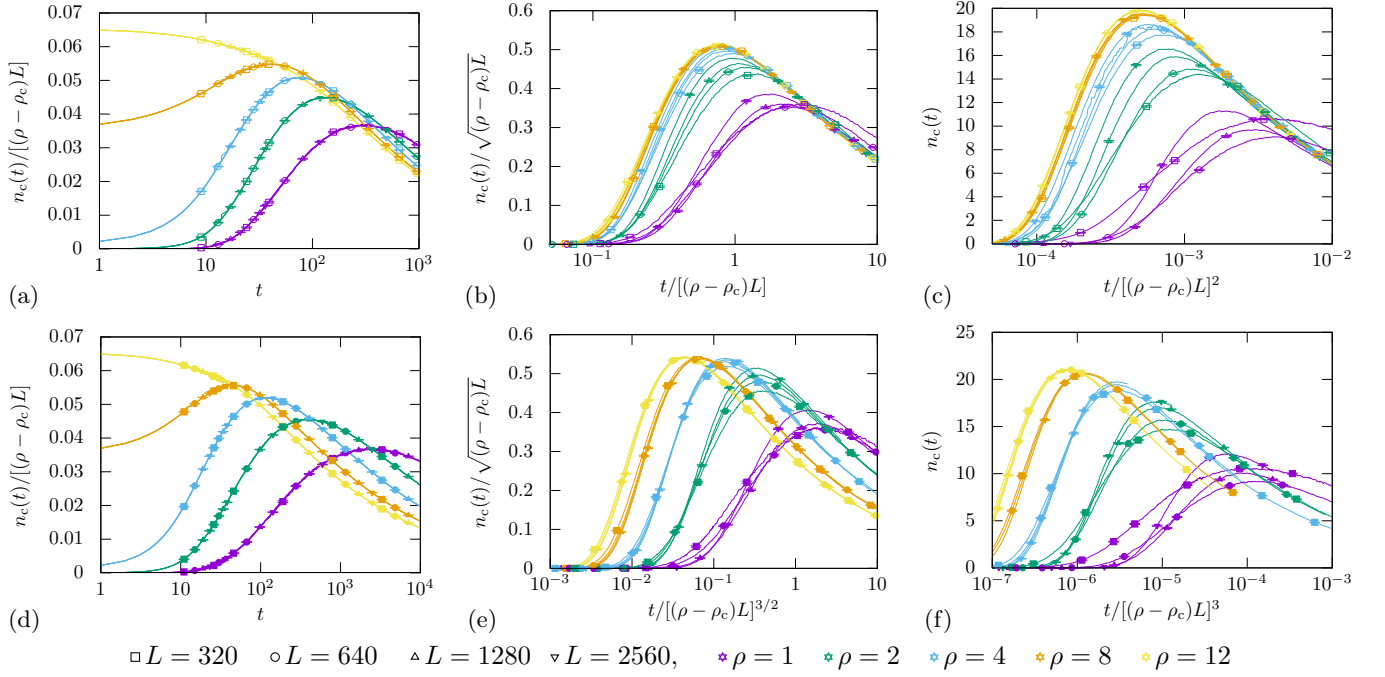


FIG. 4. Droplet counts $n_c(t)$ for the ZRP with $b = 5$ in the nucleation regime for thresholds in the droplet mass that are constant [$m_{t,\text{const}} = 10$ in (a), (d)], grow as the square root [$m_{t,\text{sqrt}} = \sqrt{(\rho - \rho_c)L}$ in (b), (e)] of, or linearly [$m_{t,\text{lin}} = (1/40)(\rho - \rho_c)L$ in (c), (f)] to the total number of particles. Results for totally asymmetric dynamics ($p_{\text{left}} = 1$) are shown with empty symbols in the top row, those for symmetric dynamics ($p_{\text{left}} = 1/2$) with filled symbols in the bottom row. Symbols represent the different system sizes $L = 320, 640, 1280$, and 2560 , colours indicate different particle densities $\rho = 1, 2, 4, 8$, and 12 . For readability symbols are only sparsely plotted and mark the corresponding lines that fully reflect the available data. The resulting time scales on the x-axis roughly correspond to the heuristic approximation.

As for the ZRP, we also consider a typical droplet mass, that we merely choose somewhat larger as $m_{t,\text{const}} = 20$ instead of estimating the critical droplet size using the bulk particle distribution given in Ref. [23] and taking the much more involved particle exchange at the droplet boundaries into account.

Due to the need of a separating site between individual droplets to distinctly count them, the initial preparation must be carried out with care, as a uniform distribution of particles easily leads to the identification of a number of large droplets in the initial configuration. This effect is visible as a small peak before the larger droplet-count maximum in Fig. 5(a,d). To eliminate this influence on the scaling exponents, we cross-checked our results using different preparation schemes. While there is an influence on the form of the droplet-count function $n_c(t)$, the effect on the rescaling exponent is negligible.

Figure 5 shows rescaled droplet counts determined for totally asymmetric as well as symmetric dynamics and averaged from 1200 individual trajectories. Except for the constant droplet-mass threshold, the obtained data collapse for the system sizes that were feasible to simulate is less convincing than for the ZRP. Due to the extension of droplets, the finite-size effects are much stronger for the PFSS.

The observed scaling exponents with thresholds $m_{t,\text{lin}}$

TABLE I. Estimated values of the scaling exponents δ_{nuc} of the typical nucleation time for the ZRP and PFSS models with totally asymmetric and symmetric dynamics, respectively.

| | $m_{t,\text{const}}$ | $m_{t,\text{sqrt}}$ | $m_{t,\text{lin}}$ |
|--|----------------------|---------------------|--------------------|
| ZRP δ_{nuc} for $p_{\text{left}} = 1$ | 0 | 1 | 2 |
| ZRP δ_{nuc} for $p_{\text{left}} = 1/2$ | 0 | 3/2 | 3 |
| PFSS δ_{nuc} for $p_{\text{left}} = 1$ | 0 | 3/2 | 5/2 |
| PFSS δ_{nuc} for $p_{\text{left}} = 1/2$ | 0 | 2 | 7/2 |

and $m_{t,\text{sqrt}}$ for the PFSS model, as given in Table I, are larger by $1/2$ with respect to those determined for the ZRP. From the heuristic approximation, one could arguably expect a small decrease in the exponents, as the distance particles need to travel to a nuclei is reduced by the droplets' spatial extension. For the constant threshold droplet mass $m_{t,\text{const}}$ we again observe a nearly perfect data collapse without any rescaling in time at all as for the ZRP. We thus obtain $\delta_{\text{nuc}} = 0$ as the nucleation exponent independent of the strength of the external drive p_{left} .

Again, as for the ZRP, we would like to emphasize that this variety of time scales depends on the choice of the typical droplet mass. For a meaningful time scale, this threshold must be selected carefully.

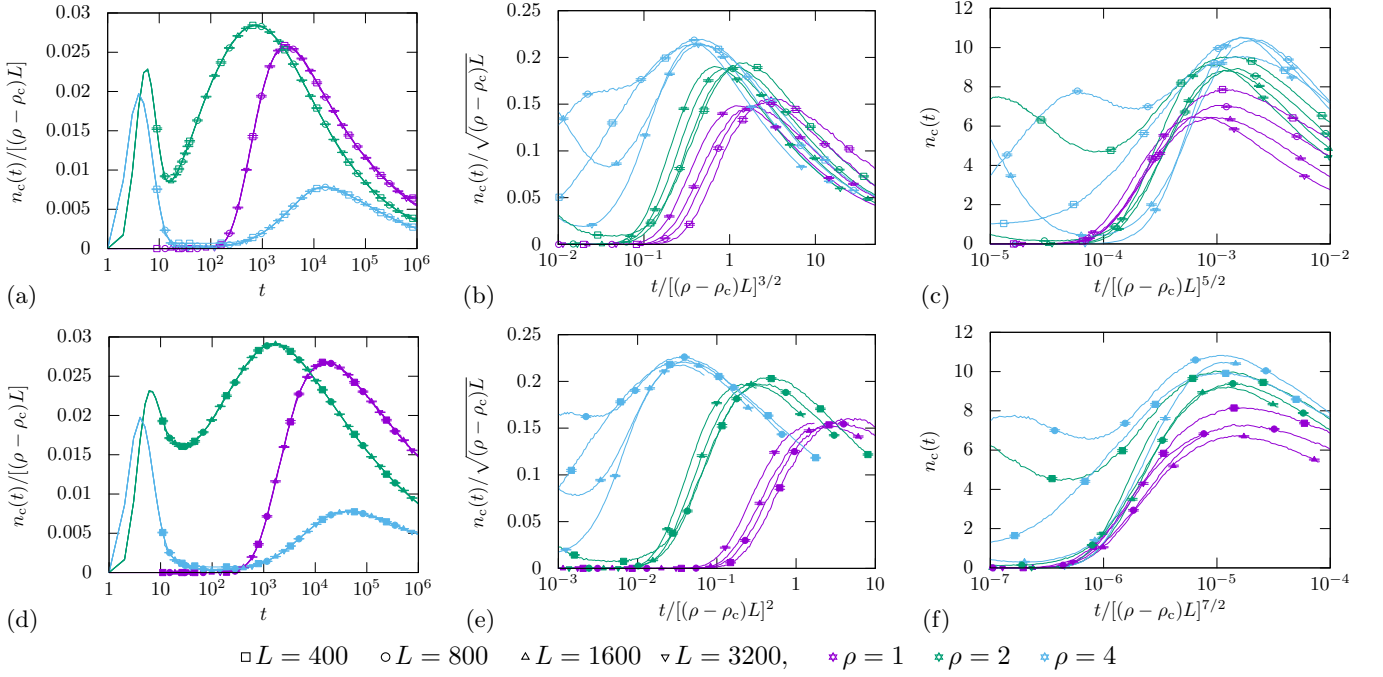


FIG. 5. Droplet counts $n_c(t)$ for the PFSS with $U = J = 1$ in the nucleation regime for thresholds in the droplet mass that are constant [$m_{t,\text{const}} = 20$ in (a), (d)], grow as the square root [$m_{t,\text{sqr}} = (5/2)\sqrt{(\rho - \rho_c)L}$ in (b), (e)] of, or linearly [$m_{t,\text{lin}} = (1/20)(\rho - \rho_c)L$ in (c), (f)] to the total number of particles. Results for totally asymmetric dynamics ($p_{\text{left}} = 1$) are shown with empty symbols in the top row, those for symmetric dynamics ($p_{\text{left}} = 1/2$) with filled symbols in the bottom row. Symbols represent the different system sizes $L = 400, 800, 1600$, and 3200 , colours indicate different particle densities $\rho = 1, 2$, and 4 .

V. COARSENING

After the relaxation of the bulk system and formation of droplet nuclei the coarsening stage dominates the kinetics. The droplets in the system exchange particles through the bulk. Because larger droplets emit less particles than smaller ones, the former grow while the latter slowly evaporate and eventually disappear. As there are fewer remaining droplets, the difference of the evaporation rates becomes smaller compared to the droplet mass and the distance of particle exchange grows. For the ZRP, the droplet evaporation rate is directly given by the hopping rate function so that the coarsening time scale can be determined quantitatively as $\delta = 2$ for totally asymmetric and $\delta = 3$ for symmetric dynamics [35].

We will consider the case of the ZRP for totally asymmetric and symmetric dynamics only to validate our methods and additionally determine the scaling exponents for the coarsening time in the situation of partially asymmetric dynamics for $0.5 \leq p_{\text{left}} \leq 1$. We will then proceed to determine the scaling exponents for the expected coarsening time in the PFSS model for asymmetric and symmetric dynamics $0.5 \leq p_{\text{left}} \leq 1$.

In the remaining section, we will first describe the considered methods to determine these scaling exponents and then discuss the respective results for the ZRP as well as the PFSS.

A simple method to estimate the coarsening time for a single trajectory is to compare the mass of the largest condensate with a threshold at the expected value of the excess mass M' . The time of first passage above this threshold from an initial state is recorded as one measurement of condensation time. The threshold value must be chosen slightly below the expected mass of the final condensate M' , so that the influence of mass fluctuations is reduced. The coarsening times τ_c are measured for each trajectory and finally averaged to determine the mean value for a given set of parameters M and p_{left} . Although being simple and fairly robust, this method does provide only limited insight into the coarsening process.

For the second method we consider the full trajectory of the relaxation process to estimate the time scale. For each simulation we record the growth of the largest droplet in terms of its mass $\overline{M}'(t)$ as a function of simulation time. The quenched average of the droplet-growth functions then directly reflects the state of the relaxation process. By rescaling $\overline{M}'(t)$ on the mass as well as the time axis we can then determine the coarsening time scale. The mass is rescaled by the expected value of excess in the steady state $\overline{M}'(t \rightarrow \infty)$ and the time is rescaled by the proposed power law (6). If the proposed scaling law holds, the scaling exponent δ can be determined by collapsing the rescaled droplet growth functions for different sizes of the system to a master curve. The

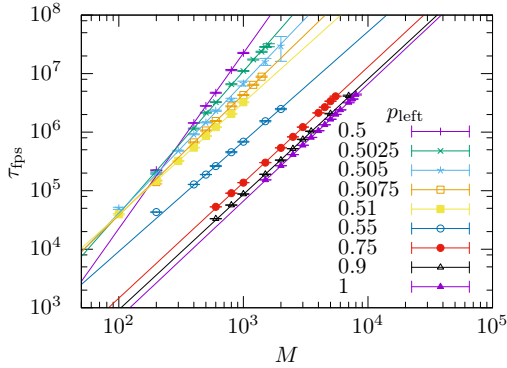


FIG. 6. Estimation of the coarsening time-scale exponent δ_{fps} for the ZRP using the first-passage method with scaling ansatz (6).

upper inset in Fig. 2 shows the result of such a collapse. To improve stability and error estimation, we perform this rescaling method over all pairs of trajectories to find the scaling exponent δ that yields the best collapse.

A. ZRP

We estimate the time scale of the coarsening process for particle density $\rho = 1$ and several values of the hopping asymmetry p_{left} to observe the transition of randomly hopping to driven particles. Here we present our results determined by the method of first-passage times as well as rescaling the function of the largest droplet mass $M'(t)$ versus time as those proved to be the most robust of the considered methods [39]. The estimates presented in this section are obtained from 10^3 to 10^4 individual simulations of the condensation process for different system sizes between 100 and 1000 sites (8000 for totally asymmetric dynamics) and the various strengths of asymmetric dynamics $1/2 \leq p_{left} \leq 1$.

The coarsening times estimated by the first-passage scaling method are given in Fig. 6. The scaling exponents of the observed pronounced power-law dependence of the coarsening time τ_{fps} to the total number of particles $M = \rho L$ are very close to the value $\delta_{fps} = 1.999 \pm 0.008$ for totally asymmetric dynamics for any sufficiently strong partial asymmetric hopping $p_{left} > 0.51$. For nearly symmetric dynamics $0.5 \leq p_{left} \leq 0.51$, a transition is observed in the exponent of the coarsening time scale as it grows to $\delta_{fps,sym} = 2.998 \pm 0.016$. The specific numerical values of the determined scaling exponents of the typical coarsening time δ_{fps} are given in Table II.

We also determined the coarsening time scale exponent by rescaling the time series of the largest droplet's mass $M'(t)$. The obtained rescaled and collapsed data for the ZRP is shown in Fig. 7. For any strength of asymmetric hopping, the curves of the rescaled mass of the largest droplet are collapsed by minimizing the square differences pair-wise for different system sizes. To find the coarsen-

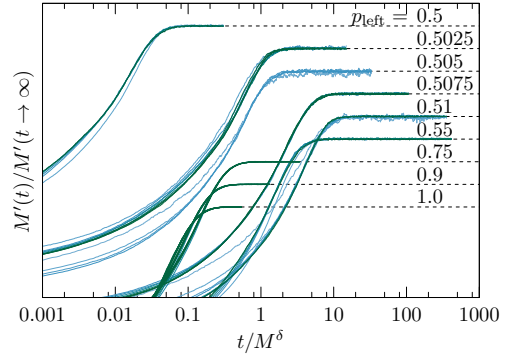


FIG. 7. ZRP coarsening: Overview of rescaled largest condensate mass trajectories fitted to collapse to master curves in the final coarsening dynamics. Groups of curves with identical strength of asymmetry are shifted on the vertical axis for readability as indicated by the right-hand side labels for the strength of asymmetric dynamics p_{left} . Curves coloured from blue to green correspond to time series of smaller (from $L = 100$) to larger (towards $L = 1000$ for symmetric and partially asymmetric and 8000 for totally asymmetric dynamics) systems with overall density $\rho = 1$. Each curve is computed from 10^4 trajectories.

TABLE II. Comparison of differently obtained scaling exponents of the coarsening time δ for various strengths of asymmetric dynamics $1/2 \leq p_{left} \leq 1$ with the numerical values of Grosskinsky et al. [35]. To compute these values, we used from 10^3 to 10^4 trajectories of systems of size $L = 100$ up to 1000 sites (8000 for totally asymmetric hopping) with an overall density of $\rho = 1$.

| p_{left} | δ_{fps} | $\delta_{M'}$ | $\delta_{Grosskinsky2003}$ |
|------------|-------------------|---------------------|----------------------------|
| 1.0 | 1.999 ± 0.008 | 2.0082 ± 0.0052 | 1.946 ± 0.019 |
| 0.9 | 2.089 ± 0.106 | 1.993 ± 0.006 | |
| 0.75 | 2.060 ± 0.098 | 1.989 ± 0.005 | |
| 0.55 | 1.891 ± 0.030 | 2.020 ± 0.046 | |
| 0.51 | 2.035 ± 0.036 | 2.035 ± 0.037 | |
| 0.5075 | 2.065 ± 0.017 | 2.102 ± 0.018 | |
| 0.505 | 2.197 ± 0.029 | 2.369 ± 0.032 | |
| 0.5025 | 2.539 ± 0.041 | 2.621 ± 0.041 | |
| 0.5 | 2.998 ± 0.016 | 3.008 ± 0.010 | 2.994 ± 0.036 |

ing time, this data collapse is performed at the end of the coarsening stage, when the largest droplet's stationary mass is approached (see the upper inset for coarsening in Fig. 2). The scaling exponents determined from the good data collapse shown in Fig. 7 are given in Table II. Additionally we can observe the different values of the constant prefactors a in the scaling law (6). For asymmetric dynamics, the coarsening time scale is roughly an order of magnitude faster for strongly asymmetric dynamics $p_{left} \leq 0.75$ compared with weakly asymmetric dynamics. For nearly and fully symmetric dynamics $p_{left} > 0.5$, however, the value of this prefactor decreases as the curves shift to the left and the scaling exponent approaches the value $\delta_{M'} = 3$. A plot of the coarsening exponents for different strengths of asymmetric dynam-

ics (see Fig. 10 below) shows a small transition region for $p_{\text{left}} \gtrsim 0.5$ where the observed scaling exponents change from $\delta = 3$ to $\delta \approx 2$. Finally, comparing our results to the literature (see Table II), we find that our methods work sufficiently well to proceed to the PFSS model.

B. PFSS

For the PFSS model with short-range interactions we estimate the exponents of the coarsening time scale δ_{fps} using the first-passage time method and $\delta_{M'}$ by rescaling the time series of the largest droplet mass as discussed above. Because of the higher computational cost to simulate this process we limited our simulations to somewhat smaller system sizes of $L = 1000$ sites for symmetric and partially asymmetric hopping and $L = 4000$ for asymmetric hopping. Our results for the coarsening times as determined by the first-passage method are given in Fig. 8. Again, the power-law time scaling is quite pronounced and the scaling exponents are easily determined as the slope of the curves as $\delta_{\text{fps}} = 2.027 \pm 0.040$ for totally asymmetric and $\delta_{\text{fps}} = 2.943 \pm 0.070$ for symmetric dynamics.

Here we also determine the numeric values of the scaling prefactor a_{fps} to the assumed power law (6) of the coarsening time scale. The specific values for different strengths of asymmetric dynamics p_{left} are given along with the respective scaling exponents in Table III. As for the ZRP, the constant prefactors increase significantly towards weaker asymmetric dynamics. We were not able to perform sufficient simulations for significantly weaker asymmetric dynamics $0.5 < p_{\text{left}} < 0.51$ due to the increasing computation costs and thus did not observe a continuous transition from asymmetric to symmetric dynamics.

The rescaled and collapsed curves determined using our second method are given in Fig. 9 and yield coarsening exponents $\delta_{M'} = 2.005 \pm 0.038$ and $\delta_{M'} = 2.855 \pm 0.031$ for totally asymmetric and symmetric dynamics, respectively. The full set of exponents for different strengths of partially asymmetric dynamics p_{left} is given in Table III. For the PFSS model the collapse shown in Fig. 9 is less distinct for the smaller system sizes of $L = 100$ sites than for the larger sizes $L \geq 200$. Although this rescaling process to collapse curves and determine the exponent by the rescaling parameter is rather involved this method yields much more stable and somewhat more robust results than the first-passage method. This is a result of its implementation using pair-wise collapse of the individual trajectories of different system sizes and global minimization of the total error function of the data collapse in the final coarsening stage.

Table III and Fig. 10 summarize the results of the scaling exponents as well as the scaling prefactor a_{fps} determined by the first method.

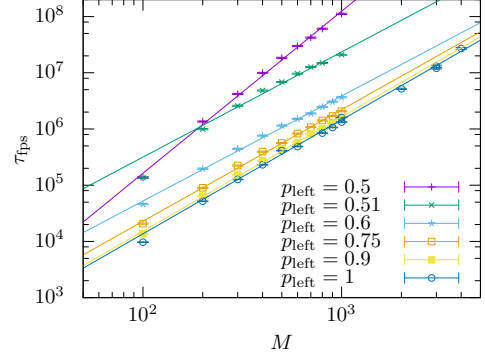


FIG. 8. Estimation of the scaling exponent δ_{fps} in the coarsening regime of the PFSS by fitting the first-passage time τ_{fps} to the assumed power law (6). The obtained values are collected in Table III.

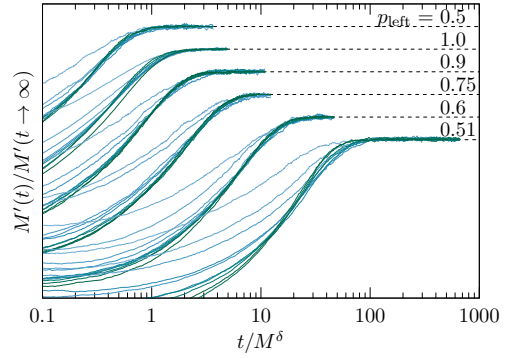


FIG. 9. PFSS coarsening: Overview of rescaled largest condensate mass trajectories fitted to collapse to master curves in the final coarsening dynamics. Groups of curves with identical values of p_{left} are shifted vertically as indicated by the right-hand side labels. Curves coloured from blue to green correspond to time series of smaller (from $L = 100$) to larger (towards $L = 1000$ for symmetric and partially asymmetric and 4000 for totally asymmetric dynamics) systems. The particle density is $\rho = 1$ for all systems. Each curve is computed from 10^4 trajectories.

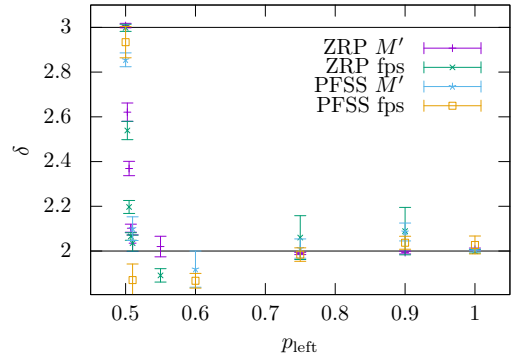


FIG. 10. Scaling exponents δ of the coarsening times versus strength of asymmetric dynamics p_{left} for both ZRP and PFSS transport processes.

TABLE III. Exponents δ_{fps} and $\delta_{M'}$ of the condensation time scale with prefactor a_{fps} for the PFSS transport model as in (6) determined by first-passage scaling (δ_{fps}) as well as pair-wise rescaling ($\delta_{M'}$) of the largest condensate mass, respectively. Values are computed from 10^4 trajectories of systems of size $L = 100$ up to 1000 sites (4000 for totally asymmetric hopping) with an overall density of $\rho = 1$. Simulations of the condensation process for higher densities $\rho = 2, 3$ yield quantitatively the same results.

| p_{left} | δ_{fps} | $\delta_{M'}$ | a_{fps} |
|-------------------|-----------------------|-------------------|------------------|
| 1.0 | 2.027 ± 0.040 | 2.005 ± 0.038 | 1.21 ± 0.31 |
| 0.9 | 2.037 ± 0.029 | 2.085 ± 0.040 | 1.28 ± 0.24 |
| 0.75 | 1.984 ± 0.030 | 2.011 ± 0.043 | 2.45 ± 0.47 |
| 0.6 | 1.867 ± 0.033 | 1.919 ± 0.081 | 9.63 ± 2.00 |
| 0.51 | 1.870 ± 0.072 | 2.100 ± 0.053 | 58 ± 26 |
| 0.5 | 2.934 ± 0.070 | 2.855 ± 0.031 | 0.28 ± 0.090 |

VI. CONCLUSIONS

In this work we considered the dynamics of the two stages, nucleation and coarsening, of the condensation process in the zero-range process (ZRP) condensation model as well as a stochastic transport process with pair-factorized steady states (PFSS) and condensation dynamics. To obtain the typical time scales of the nucleation and coarsening process, we considered the power-law scaling observed for zero-range processes with condensation dynamics and employed complementary numerical methods.

For the nucleation regime in both processes we find most notably the strong dependence of the scaling exponent of the nucleation time on the choice of the typical droplet mass that acts as a marker to the end of the regime. The determined exponents for the ZRP for the three choices of the typical droplet mass, for totally asymmetric and symmetric dynamics respectively, are $\delta_{\text{ZRP,nucl}} = 2$ and 3 for $m_{t,\text{lin}} \propto (\rho - \rho_c)L$ linear in the excess mass, $\delta_{\text{ZRP,nucl}} = 1$ and $3/2$ for $m_{t,\text{sqrt}} \propto \sqrt{(\rho - \rho_c)L}$ linear in the square root of the excess mass and $\delta_{\text{ZRP,nucl}} = 0$ for $m_{t,\text{const}}$ independent of the system size. These exponents were also expected using a simple heuristic approximation of the involved time scales. The almost perfect data collapse of the droplet-count function for the threshold based on our approximation of the critical droplet size for the ZRP suggests that indeed the assumption of a typical droplet mass $m_{t,\text{const}}$ that is an intensive variable, i.e. does not depend on the system size, is physical for the ZRP and the PFSS model as well. However, considering the versatility of these models allowing a large variety of mappings to other models, the freedom to choose the type of the droplet mass threshold with respect to such a mapping and obtain an appropriate nucleation time scale seems to be of advantage.

For the pair-factorized steady states model we determined scaling exponents using the same types of typical droplet masses with differences in the prefactors to ac-

count for the larger extended droplets. Remarkably, our obtained values of these exponents directly correspond to those of the ZRP plus a shift of $1/2$ towards longer nucleation times for the considered droplet mass thresholds that depend on the system size. The specific values, for totally asymmetric and symmetric dynamics, are $\delta_{\text{PFSS,nucl}} = 5/2$ and $7/2$ for the threshold $m_{t,\text{lin}}$ linear in the excess mass, $\delta_{\text{PFSS,nucl}} = 3/2$ and 2 for $m_{t,\text{sqrt}}$ linear in the square root of the excess mass and $\delta_{\text{PFSS,nucl}} = 0$ for the threshold $m_{t,\text{const}}$ independent of the system size.

It would be rewarding for further research to study the details of the involved nucleation processes that lead to the observed relation between the exponents for the PFSS and those of the ZRP. Furthermore, it is worth studying the crossover to the coarsening regime in stochastic transport processes in more detail.

For the coarsening time scale exponents we determined results employing two independent numerical methods. To test these, we first reproduced the scaling exponents of the ZRP determined analytically and numerically by Grosskinsky et al. [35] for symmetric as well as totally asymmetric dynamics. Our results for the scaling exponents of the coarsening times are $\delta_{\text{ZRP,tas}} = 2.0082 \pm 0.0052$ and $\delta_{\text{ZRP,sym}} = 3.008 \pm 0.010$ as well as $\delta_{\text{PFSS,tas}} = 2.005 \pm 0.038$ and $\delta_{\text{PFSS,sym}} = 2.855 \pm 0.031$ for the PFSS model, both for symmetric and totally asymmetric dynamics respectively. In contrast to the nucleation regime, the coarsening exponents of the ZRP and PFSS models match very well suggesting that, although the early condensation dynamics differ, the coarsening process in these processes is much more similar. We supplemented these values with results for partially asymmetric dynamics and showed the transition in the observed coarsening times from symmetric to predominantly asymmetric dynamics at $p_{\text{left}} \geq 0.51$ from $\delta = 3$ to 2 accompanied by a distinct change in the prefactor of the scaling. This is most likely due to the finite system size. For the PFSS in the coarsening regime we discussed results for the scaling exponents with symmetric, as well as partially and totally asymmetric dynamics. We were not able to directly observe such a transition in the coarsening exponents from $\delta = 3$ to 2 for very weakly asymmetric dynamics as for the ZRP, due to the increase in the computational costs for such parametrisations. The prefactor of the scaling, however, rapidly increases for nearly symmetric dynamics as observed for the ZRP as well.

ACKNOWLEDGMENTS

We are grateful to Johannes Zierenberg for insightful suggestions and discussions of the nucleation dynamics. We thank the DFG (German Science Foundation) for financial support under Grant No. JA 483/27-1. We further acknowledge support by the DFH-UFA Doctoral College “ \mathbb{L}^4 ” under Grant No. CDFA-02-07 as well as the EU through the Marie Curie IRSES network DIONICOS under contract No. PIRSES-GA-2013-612707.

-
- [1] F. Spitzer, "Interaction of Markov processes," *Adv. Math.* **5**, 246 (1970).
- [2] A. Garai, D. Chowdhury, D. Chowdhury, and T. V. Ramakrishnan, "Stochastic kinetics of ribosomes: Single motor properties and collective behavior," *Phys. Rev. E* **80**, 011908 (2009).
- [3] D. Chowdhury, L. Santen, and A. Schadschneider, "Statistical physics of vehicular traffic and some related systems," *Phys. Rep.* **329**, 199 (2000).
- [4] D. Chowdhury, A. Schadschneider, and K. Nishinari, "Physics of Transport and Traffic Phenomena in Biology: From molecular motors and cells to organisms," *Phys. Life Rev.* **2**, 318 (2005).
- [5] A. Schadschneider, D. Chowdhury, and K. Nishinari, *Stochastic Transport in Complex Systems* (Elsevier, Amsterdam, 2011) p. 555.
- [6] G. M. Shim, B. Y. Park, J. D. Noh, and H. Lee, "Analytic study of the three-urn model for separation of sand," *Phys. Rev. E* **70**, 031305 (2004).
- [7] D. Beysens and C. M. Knobler, "Growth of Breath Figures," *Phys. Rev. Lett.* **57**, 1433 (1986).
- [8] L. Bogacz, Z. Burda, W. Janke, and B. Waclaw, "Balls-in-boxes condensation on networks," *Chaos* **17**, 026112 (2007).
- [9] B. Waclaw, L. Bogacz, Z. Burda, and W. Janke, "Condensation in zero-range processes on inhomogeneous networks," *Phys. Rev. E* **76**, 046114 (2007).
- [10] B. Waclaw, Z. Burda, and W. Janke, "Power laws in zero-range processes on random networks," *Eur. Phys. J. B* **65**, 565 (2008).
- [11] S. Kwon and Y. Kim, "Condensation phenomena of the generalized conserved-mass aggregation model on complex networks," *Phys. Rev. E* **83**, 031132 (2011).
- [12] M. R. Evans and T. Hanney, "Nonequilibrium statistical mechanics of the zero-range process and related models," *J. Phys. A: Math. Gen.* **38**, R195 (2005).
- [13] M. R. Evans, "Phase transitions in one-dimensional nonequilibrium systems," *Braz. J. Phys.* **30**, 42 (2000).
- [14] B. Derrida, E. Domany, and D. Mukamel, "Exact diffusion constant of a one-dimensional asymmetric exclusion model with open boundaries," *J. Stat. Phys.* **69**, 667 (1992).
- [15] B. Derrida, M. R. Evans, V. Hakim, and V. Pasquier, "Exact solution of a 1D asymmetric exclusion model using a matrix formulation," *J. Phys. A: Math. Gen.* **26**, 1493 (1993).
- [16] A. B. Kolomeisky and G. M. Schütz, "Phase diagram of one-dimensional driven lattice gases with open boundaries," *J. Phys. A: Math. Gen.* **31**, 6911 (1998).
- [17] B. Derrida, "An exactly soluble non-equilibrium system: The asymmetric simple exclusion process," *Phys. Rep.* **301**, 65 (1998).
- [18] R. A. Blythe, W. Janke, D. A. Johnston, and R. Kenna, "The grand-canonical asymmetric exclusion process and the one-transit walk," *J. Stat. Mech.: Theor. Exp.* **2004**, P06001 (2004).
- [19] O. J. O'Loan, M. R. Evans, and M. E. Cates, "Jamming transition in a homogeneous one-dimensional system: The bus route model," *Phys. Rev. E* **58**, 1404 (1998).
- [20] M. R. Evans and B. Waclaw, "Condensation in models with factorized and pair-factorized steady states," *J. Stat. Mech.: Theor. Exp.* **2015**, P09005 (2015).
- [21] M. R. Evans, T. Hanney, and S. N. Majumdar, "Interaction-Driven Real-Space Condensation," *Phys. Rev. Lett.* **97**, 010602 (2006).
- [22] B. Waclaw, J. Sopik, W. Janke, and H. Meyer-Ortmanns, "Tuning the Shape of the Condensate in Spontaneous Symmetry Breaking," *Phys. Rev. Lett.* **103**, 080602 (2009).
- [23] B. Waclaw, J. Sopik, W. Janke, and H. Meyer-Ortmanns, "Mass condensation in one dimension with pair-factorized steady states," *J. Stat. Mech.: Theor. Exp.* **2009**, P10021 (2009).
- [24] E. Ehrenpreis, H. Nagel, and W. Janke, "Numerical survey of the tunable condensate shape and scaling laws in pair-factorized steady states," *J. Phys. A: Math. Theor.* **47**, 125001 (2014).
- [25] C. Godrèche and J. M. Luck, "Dynamics of the condensate in zero-range processes," *J. Phys. A: Math. Gen.* **38**, 7215 (2005).
- [26] O. Hirschberg, D. Mukamel, and G. M. Schütz, "Motion of condensates in non-Markovian zero-range dynamics," *J. Stat. Mech.: Theor. Exp.* **2012**, P08014 (2012).
- [27] P. Chleboun and S. Grosskinsky, "Finite size effects and metastability in zero-range condensation," *J. Stat. Phys.* **140**, 846 (2010).
- [28] E. Levine, D. Mukamel, and G. M. Schütz, "Zero-range process with open boundaries," *J. Stat. Phys.* **120**, 759 (2005).
- [29] H. Nagel, H. Meyer-Ortmanns, and W. Janke, "Boundary-drive-induced formation of aggregate condensates in stochastic transport with short-range interactions," *Europhys. Lett.* **111**, 30001 (2015).
- [30] H. Nagel and W. Janke, "Emergence of dynamic phases in the presence of different kinds of open boundaries in stochastic transport with short-range interactions," *J. Stat. Mech.: Theor. Exp.* **2016**, 013207 (2016).
- [31] W. Ostwald, "Studien über die Bildung und Umwandlung fester Körper," *Z. Phys. Chem.* **22**, 289 (1897).
- [32] L. Farkas, "Keimbildungsgeschwindigkeit in übersättigten Dämpfen," *Z. Phys. Chem.* **125**, 236 (1927).
- [33] R. Becker and W. Döring, "Kinetische Behandlung der Keimbildung in übersättigten Dämpfen," *Ann. Phys.* **416**, 719 (1935).
- [34] I. M. Lifshitz and V. V. Slyozov, "The kinetics of precipitation from supersaturated solid solutions," *J. Phys. Chem. Solids* **19**, 35 (1961).
- [35] S. Grosskinsky, G. M. Schütz, and H. Spohn, "Condensation in the zero range process: Stationary and dynamical properties," *J. Stat. Phys.* **113**, 389 (2003).
- [36] C. Godrèche, "Dynamics of condensation in zero-range processes," *J. Phys. A: Math. Gen.* **36**, 6313 (2003).
- [37] J. K. Ochoab, H. Nagel, W. Janke, and B. Waclaw, "A simple non-equilibrium, statistical-physics toy model of thin-film growth," *J. Stat. Mech.: Theor. Exp.* **2015**, P09013 (2015).
- [38] M. Barma and K. Jain, "Locating the minimum: Approach to equilibrium in a disordered, symmetric zero range process," *Pramana* **58**, 409 (2002).
- [39] As a cross-check, we also rescaled the average droplet count function, to obtain a data collapse at the point where only a single droplet would remain.